Cooperative Jahn-Teller effect in TmZn

P. Morin, J. Rouchy, D. Schmitt
Laboratoire Louis Néel, Centre National de la Recherche Scientifique
166X, 38042 Grenoble Cedex, France
(Received 02 May 1977)

Specific-heat, resistivity, neutron-spectroscopy, magnetization, and magnetostriction experiments on TmZn are reported. This equiatomic metallic compound crystallizes with the cubic CsCl structure and shows a first-order Jahn-Teller transition to a tetragonal structure at $T_Q = 8.55$ K. The cell distortion reaches $c/a - 1 = (-9 \pm 1) \times 10^{-3}$. The magnetic moment orders along a fourfold axis at $T_c = 8.12$ K, its value being largely field dependent. Due to the vicinity of the transitions, they are mixed and strongly raised in temperature by (even low) applied fields as observed by the magnetization and magnetostriction experiments in the paramagnetic state. These results and the elastic constants previously published are analyzed taking into account the quadrupole-quadrupole exchange and the quadrupole-lattice term beside the Heisenberg exchange and the cubic crystal electric field (CEF) terms; the CEF parameters are $A_4\langle r^4\rangle = -38 \pm 5$ K and $A_6\langle r_6\rangle = -19.6 \pm 2$ K/atom. The ground state is the magnetic triplet $\Gamma_5^{(1)}$ in the cubic paramagnetic state. The theoretical study of the dependence of T_c and T_Q on the bilinear and biquadratic exchange terms reveals a complex phase diagram. In the case of TmZn, the obtained second-order coefficients allow a good description of all the physical properties now investigated.

I. INTRODUCTION

The equiatomic compounds *R*Zn of the rare earths with zinc crystallize with the cubic CsCl-type structure.[1] Various measurements on both single-crystals and polycrystalline samples have been performed including magnetization,[2] specific-heat,[3] and neutron-spectroscopy[4] experiments. A main result for this metallic series is that the high degree of simplicity of the cubic structure with only one magnetic ion per cell is strongly complicated by its inclination to be strained by a magnetostrictive process. The modulation of both one-ion and two-ion terms of the Hamiltonian by the lattice distortions has been recently investigated through all the series, proving strong quadrupole-strain effects.[5]

On the other hand, the effect of the crystalline electric field (CEF) was shown to be important. The CEF parameters A_4 and A_6 are negative, varying across the *R*Zn series in a complicated way, far from any point-charge model estimates.[4] The large $5d$ character (e_g type) of the conduction band predicted by band calculations[6] induces the main contributions to the CEF parameters, that are direct and exchange Coulombic ones.

In addition to the Heisenberg interaction, local coupling between the $4f$ shell and the conduction band contributes to anisotropic exchange terms like biquadratic ones and the magnetic interactions are not well described by a simple indirect Ruderman-Kittel-Kasuya-Yosida model. The analysis of the magnon dispersion curves[7] on HoZn led to two main conclusions: (i) the same second-order terms (magnetoelastic and/or quadrupolar) in the Hamiltonian are necessary to fit both spin-wave and magnetization curves; (ii) the Heisenberg interactions between the first rare-earth neighbors and the third ones have been found preponderant.

TmZn is unique in the series. Due to the weak magnetic interactions one may observe other characteristic two-ions or one-ion terms. Ultrasonic experiments have recently revealed strong magnetoelastic effects in addition to an exchange coupling between $4f$ quadrupoles.[8] Due to the lack of definitive experiments, it was considered a magnetostrictive compound, not a Jahn-Teller material like isomorphous TmCd.[9]

The purpose of this paper is to present in Sec. II new experiments (specific heat, resistivity, neutron spectroscopy, magnetization, and strain) showing that its situation is more complex. It exhibits two separate order parameters, the quadrupolar one is associated with a cubic-tetragonal transition occuring at higher temperature than the ferromagnetic Curie point, TmZn being then a Jahn-Teller compound. In Sec. III, an analysis of all the results is presented using a Hamiltonian taking into account all the second-order terms in a molecular-field approximation.

II. EXPERIMENTS

TmZn samples were obtained by the direct fusion of the two components in stoichiometric preparations in a sealed tantalum crucible. The crystal growth was per-

formed in a Bridgman furnace with a temperature gradient of about 20 °C/cm.

A. Specific heat

We have used an ingot of about 30 g. It has been checked by etching and x rays to be monocrystalline, that assures the best homogeneity and thermal conductivity. The heat-capacity measurements were performed in an adiabatic calorimeter at the Services des Basses Températures of the Centre d'Etudes Nucléaires in Grenoble. The sample was fixed by copper clips and isolated from the calorimeter. The temperature was measured by means of carbon resistance thermometer calibrated with an accuracy of 10^{-3} K, and the precision on the specific-heat values is better than 2%.

The results obtained at low temperature are given in Fig. 1. Two peaks of different natures are observed at $T_c = 8.12 \pm 0.01$ K and $T_Q = 8.55 \pm 0.01$ K. The second transition appears to be a very narrow first-order one, the maximum value of C_p being of about 270 J/(K mole) (in comparison, the lattice contribution remains at about 50 J/(K mole) at room temperature). The evaluation of the latent heat from the first-order peak area (or from the entropy gap at T_Q) leads to a value of 19 ± 1 J/mole. But these values are strongly correlated with the quality of the sample.

The lower transition observed at 8.12 K seems to be of second order. Both reveal the existence of two order parameters; T_Q is associated with the ordering of the $4f$ quadrupole and the magnetic moments order at the Curie temperature T_c. The value of T_Q could not be evaluated (in earlier ultrasonic work) from the extrapolation of the drastic thermal variation of the $C_{11} - C_{12}$ soft mode,[8] because the echoes vanished at about 13 K, due to the strong attenuation. The value of $T_c = 8.12$ K differs from the first rough determination of 10 K,[8] but has been confirmed during the new magnetic experiments presented below.

Both transitions can be described by a power law:

$$C^p = A\,[(T - T^*)/T^*]^{-\alpha}\,.$$

Taking into account background effects, a least squares fit led for the high-temperature side of T_Q to $\alpha = +0.9 \pm 0.1$ and $T_Q{}^* = 8.55 \pm 0.03$ K. For the low-temperature side of T_c, α was found to be about +0.3.

In the thermal range of Fig. 1, the lattice and electronic contributions to the entropy and the copper clips ones are less than 0.2 J/K for 1 mole of TmZn. Above T_Q the specific heat developed originates mainly from CEF effects.. But extending the measurements up to 40 K did not reveal any large Schottky anomaly.

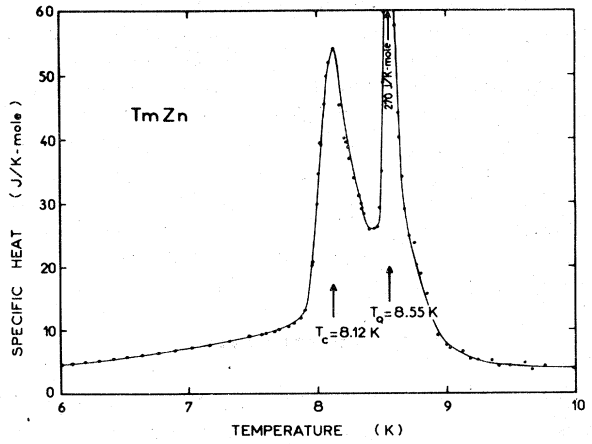

FIG. 1. Specific heat of TmZn; T_c is the magnetic ordering temperature, T_Q the structural transition one.

B. Resistivity measurements

The change of the electrical resistivity at the quadrupolar ordering can confirm the specific-heat results. Resistivity measurements were performed on two rods. The first one was spark cut from the monocrystalline ingot used for the specific-heat and neutron-spectroscopy experiments. The second one originates from the same monocrystalline ingot that was used for magnetization, magnetostriction, and elastic-constants measurements. In both cases, the rod was not oriented along a particular crystallographic axis, but was verified by etching and x rays to be monocrystalline.

Figure 2(a) shows the thermal variation of the resistivity $\rho(T)$ and its derivative $\rho'(T)$ for the first sample. It shows clearly two transitions in good agreement with the specific-heat data. When cooling and heating the sample, a perfect reproductibility is obtained at the lower temperature (8.1 K), corresponding to the magnetic ordering, but we observed both latent heat and hysteresis at the first-order one ($T_Q = 8.5$ K). We can note that the $\rho'(T)$ derivative exhibits roughly the same behavior as the specific-heat curve. This experiment proves that the specific-heat ingot does not include any parasitic internal crystallite which might order at a different temperature and hence be responsible for one of the two observed peaks.

On the second sample we did not observe a well-marked step between the two transitions, but a latent heat and an hysteresis appeared [Fig. 2(b)]. On the ρ' curve, the two peaks are not resolved leading to a roughly constant step of about 0.3 K, the transitions being closer to each other. We have verified that this behavior is strongly different from that observed in ErZn, where the magnetic ordering appears at 20 K accompanied by a magnetostrictive process. On a monocrystalline rod of this compound, we observed

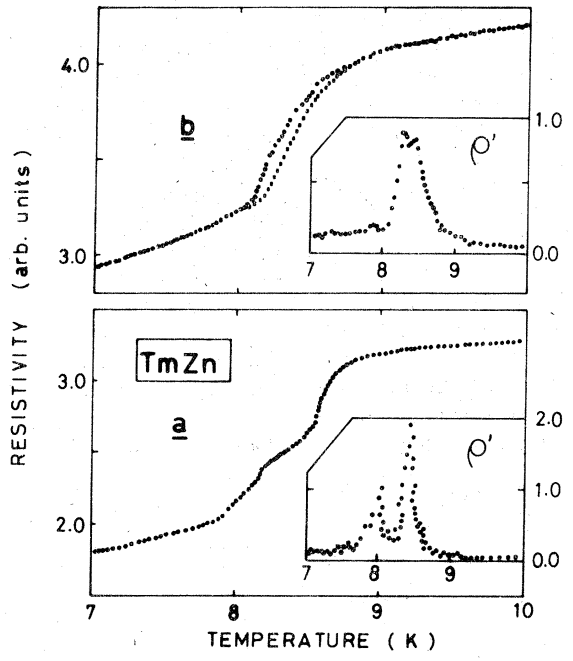

FIG. 2. Thermal variation of the resistivity and its derivative in the transition range. (a): for the rod cut from the C_p ingot (b): for the other sample. •: experimental points obtained when decreasing the temperature. □: when increasing it.

only a smooth change on the ρ curve at T_c, without hysteresis. The ρ' curve exhibited a λ anomaly like the specific-heat one, as reported for instance for GdSb,[10] its value remaining (at T_c) 10 times lower than in TmZn. If the T_c and T_Q temperatures were mixed, we would observe only a narrow first-order transition as in HoSb.[10] The ρ' full width at half-maximum for the second TmZn sample is about 0.45 ± 0.1 K instead of 0.1 K as observed for the first rod or in HoSb. We conclude that the sample preparation can modify the ordering, the structural transition temperature being the most sensitive one. In the case of the latter ingot, which is the oldest one, its quality can be influenced by a rougher art of crystal growth.

C. Neutron spectroscopy

The most direct determination of the crystal field is achieved in the paramagnetic range by neutron spectroscopy. As previously,[4] the experiments were performed on the IN7 time-of-flight spectrometer at the Institut Laue-Langevin in Grenoble. The incident energy ranged from 8.95 to 46.8 meV, depending on the different energy transfers investigated. The spectra are dominated by an intense elastic line, the width of which never exceeded the instrumental resolution (about 2.0 meV for an incident energy of $E_0 = 35.8$ meV). The observed widths for inelastic lines are generally slightly smaller. Assuming Gaussian shapes, we may deduce that natural transition widths are in the range of 0.5–1.5 meV.

Spectra were taken at different temperatures. The lower temperature was fixed slightly above the two transition points to observe only excitation processes from the lowest cubic levels. The higher temperatures were chosen in order to populate excited levels and to observe new transitions by excitation and/or deexcitation processes.

Some characteristic spectra are reported in Figs. 3 and 4. At 12 K, beside the $E_0 = 25.4$ meV elastic line [Fig. 3(a)], there appears two strong inelastic lines associated with transfers of 3.2 and 13.9 meV (i.e., 37 and 161 K). Despite the low temperature, the smaller one can be observed by deexcitation process as the nonresolved line on the left-hand side of the elastic peak. In order to better the resolution for large transfers, a spectrum was taken at $E_0 = 46.8$ meV [Fig. 4(a)]. It reveals peaks of small intensity at 17.3 and 22.6 meV (i.e., 201 and 262 K). At 32 K, the deexcitation process from the level lying at 37 K increases as proved by the Fig. 3(b) ($E_0 = 8.95$ meV). At 120 K, where many levels are populated, the deexcitation lines from the levels lying at 37, and 161 K increase

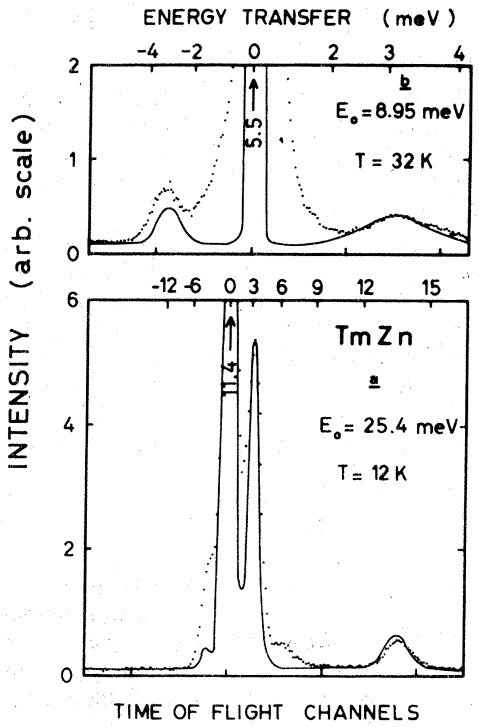

FIG. 3. Time of flight spectra for TmZn at (a) $T = 12$ K, $E_0 = 25.4$ meV and (b) $T = 32$ K, $E_0 = 8.95$ meV. Solid lines are theoretical fits.

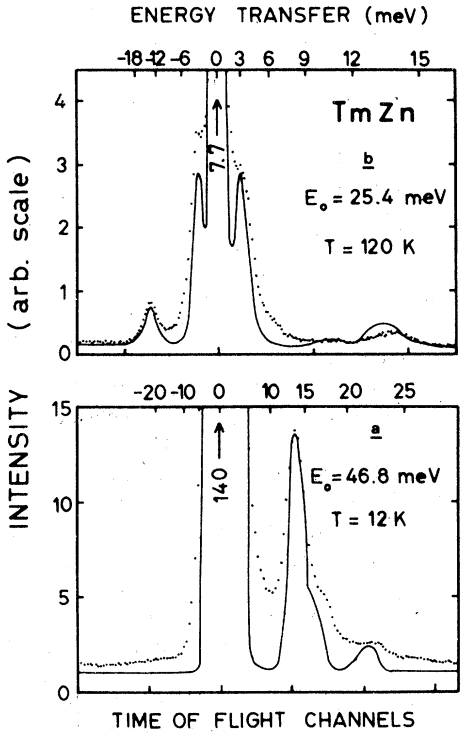

FIG. 4. Time of flight spectra for TmZn at (a) $T = 12$ K, $E_0 = 46.8$ meV and (b) $T = 120$ K, $E_0 = 25.4$ meV. Solid lines are theoretical fits.

strongly [Fig. 4(b)], proving that they arise from CEF transitions. Besides, previous studies on nonmagnetic YZn have shown that phonon lines do not appear in these experimental conditions. Theoretical fits will be presented in Sec. III.

In addition, we have tried to obtain information on the splitting of the lowest states in the tetragonal phase. As it would be difficult to collect data between T_c and T_Q, we preferred to follow the thermal dependence of the 3.2 meV line down to 4.2 K even if we were involved with q-integrated spin wave excitations below T_c. At T_Q we observed a sudden decrease of the transfer toward 2.3 meV, this value remaining then roughly constant.

D. Magnetic measurements

Monocrystalline spheres about 3 mm in diameter were spark cut and used for magnetic measurements along the three principal crystallographic axes. The experiments were performed at the Service National des Champs Intenses at Grenoble in fields available up to 150 kOe. First, we made accurate measurements of the thermal variation of the magnetization in weak fields. The Curie point was found to be 8.0 ± 0.1 K and no discontinuity in the susceptibility was observed at T_Q due to the vicinity of both ordering points. The three principal magnetization curves at low temperature (1.3 K) have been already reported in Ref. 8.

We present here the curves obtained along the fourfold axis for different temperatures from 1.3 up to 32 K [Fig. 5(a)]. Above T_c, the monocrystalline sample exhibits a sudden transition from a paramagnetic state to a ferromagnetic single domain one at a critical field H_c. The strength of its hysteresis depends on the field variation rate. The magnetization curves become smoother at higher temperatures which leads to larger uncertainties in the determination of H_c. The thermal dependence of H_c is reported in the inset of Fig. 5(a). The internal energy variation at the critical field can be evaluated by applying the Clausius-Clapeyron relation for the associated variables M and H,

$$L = T(M_2 - M_1)\frac{dH}{dT},$$

where $M_2 - M_1$ is the magnetization jump and

$$\frac{dH}{dT} \simeq 2.8 \text{ kOe/K}$$

can be deduced from the thermal variation of H_c. The largest uncertainties in the L values are due to

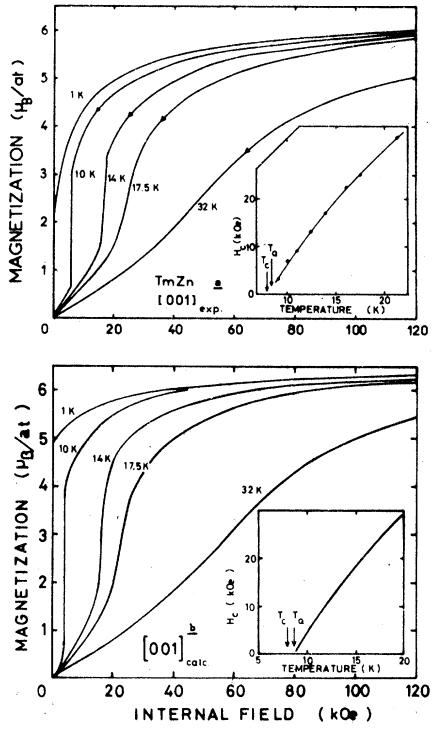

FIG. 5. Magnetization curves of TmZn along the [001] axis at different temperatures; the insets show the temperature dependence of the critical field H_c. [(a) experimental; (b) calculated].

uncertainty in the $M_2 - M_1$ gap. In the first 6-K range, the latent heat is found of about 28 ± 5 J/mole, that is larger than for the lattice transition at T_Q (Sec. II A).

The set of magnetization curves obtained with the field applied along the twofold axis presents a similar behavior [Fig. 6(a)]. First a large anisotropy of the magnetization appears at low temperature: 25% in 40 kOe and 17% in 100 kOe of the value along the fourfold axis. Calculations will explain that this is due to the rotation process of the moment to the twofold field direction and to the anisotropic purification of the ground-state wave function. In the paramagnetic state, the susceptibility is verified to be anisotropic too. In low field we obtained a value of about 94% of the fourfold easy axis one. The jump of the magnetization curves occured for field values nearly twice as large as those along the easy direction. This is larger than expected by a simple analysis, which leads to a ratio $\sqrt{2}$, the transition occuring when the field component along the fourfold axis, $H_{[101]}/\sqrt{2}$ reaches the critical value $H_{c[001]}$. With slow field variations, we have been able to reduce the hysteresis as was the case for the fourfold axis.

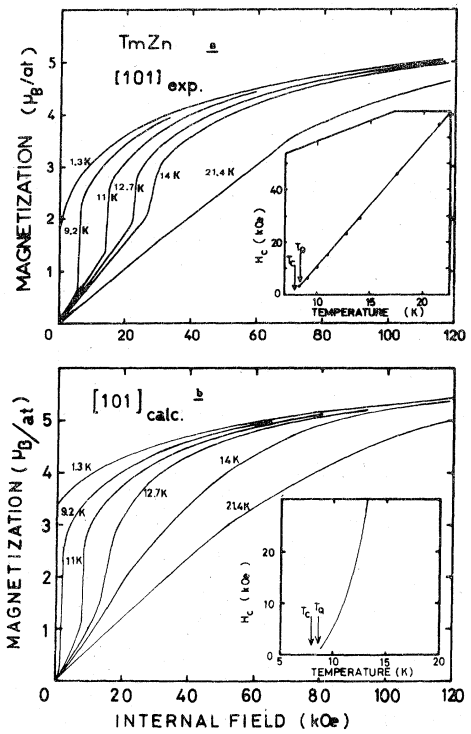

FIG. 6. Magnetization curves of TmZn along the [101] axis at different temperatures. The insets show the temperature dependence of the critical field H_c.

E. Strain data

The study of the tetragonal strain has been performed by means of Micromeasurements (350-Ω) electrical resistance strain gauges in the 12-kOe field provided by an electromagnet. Flat disks were spark cut parallel to a fourfold crystallographic plane; the samples were about 10 mm in diameter and 1 mm thick, the field being large enough to observe the spontaneous strain. For better accuracy, we used two active gauges bonded along the two perpendicular fourfold axes. A standard one was bonded on a silica sample. Both sets of values, for the difference

$$\lambda_{\parallel} - \lambda_{\perp} = c/a - 1$$

between measurements parallel and perpendicular to the field applied along a fourfold axis, were always in agreement to better than 3% and yielded the spontaneous tetragonal strain in the ordered state and the field induced one in the paramagnetic range.

The tetragonal strain versus the magnetic field is reported in Fig. 7(a). At low temperature the spontaneous strain can be observed after the domain's disappearance under field. The strain appears to be field dependent, increasing from a spontaneous value of about

$$c/a - 1 = (-9 \pm 1) \times 10^{-3} .$$

In the paramagnetic state, the same behavior is observed as reported for the paramagnetic moment (Figs. 5 and 6). The sample changes from a cubic structure weakly strained by the normal parastriction process to a quadratic single domain at a critical field which depends on the temperature. The thermal dependence of the critical field is about 4 kOe/K immediately above T_Q, before approaching, at higher temperature, the same 2.8 kOe/K value as for magnetization data (inset of Fig. 8). We have reported in Fig. 8 two sets of measurements with different rates of

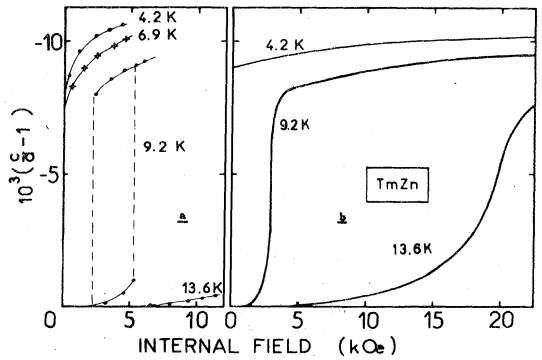

FIG. 7. Tetragonal strain curves of TmZn at different temperatures [(a) experimental; (b) calculated].

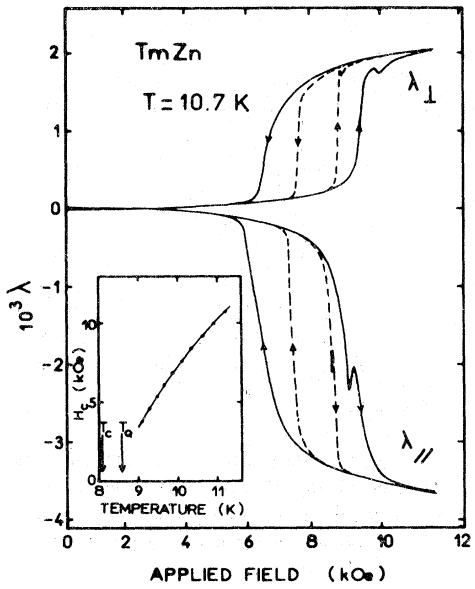

FIG. 8. Experimental variations of the strains parallel ($\lambda_{\parallel}$) and perpendicular ($\lambda_{\perp}$) to the applied field fourfold direction at 10.7 K. Full and dashed lines are relative to fast and slow rates of the increasing field. The inset shows the temperature dependence of the critical field H_c.

increasing field; the hysteresis of the transition is reduced with the slow rate (about 0.3 kOe/mm instead of 3 kOe/mm). The small anomaly during the transition may be correlated to the latent heat developed and temperature inhomogeneities in the sample. A similar behavior has been observed for measurements of the magnetization in low fields in function of the temperature.

III. INTERPRETATION OF THE RESULTS

A. Formalism

The interpretation of our experimental results is based upon the use of the following Hamiltonian in the molecular-field approximation (MF):

$$\mathcal{H} = \mathcal{H}_{\mathrm{CEF}} - g\mu_B(\vec{H}_{\mathrm{ex}} + \vec{H}_i)\cdot\vec{J} + \mathcal{H}_{qq} + \mathcal{H}_{\mathrm{me}} \ , \qquad (1)$$

$$H_{\mathrm{CEF}} = Wx(O_4/F_4) + W(1-|x|)(O_6/F_6)$$

is the Lea, Leask, and Wolf (LLW) form for the cubic CEF Hamiltonian[11] expressed in fourfold axes;

$$\vec{H}_{\mathrm{ex}} = 3\Theta_p\langle\vec{J}\rangle/J(J+1)g\mu_B$$

is the molecular field evaluated from the ordering temperature ($\Theta_p = 8.1$ K); $\vec{H}_i$ is the internal field (applied field corrected for the demagnetization effects); $\mathcal{H}_{qq}$ is the biquadratic exchange Hamiltonian[12] in the molecular-field approximation

$$\mathcal{H}_{qq} = -K_1(\langle O_2^0\rangle O_2^0 + 3\langle O_2^2\rangle O_2^2) - 4K_2(\langle P_{xy}\rangle P_{xy} + \langle P_{yz}\rangle P_{yz} + \langle P_{zx}\rangle P_{zx}) \ , \qquad (2)$$

where O_2^0, O_2^2, and P_{ij} are the second-order Stevens' operators

$$O_2^0 = 3J_z^2 - J(J+1) \ , \quad O_2^2 = J_x^2 - J_y^2 \ ,$$

$$P_{ij} = \tfrac{1}{2}(J_iJ_j + J_jJ_i) \ , \quad ij = xy,yz,zx$$

$\mathcal{H}_{\mathrm{me}}$ is the magnetoelastic Hamiltonian limited to the one-ion term (second-order CEF term) linear in strain. Here are neglected the modification of the fourth- and sixth-order terms, the two-ion magnetoelastic contributions and the anharmonic terms. This simplifying hypothesis will be discussed in Sec. III C 3.

$$\mathcal{H}_{\mathrm{me}} = -B_1(\epsilon_3 O_2^0 + \sqrt{3}\epsilon_2 O_2^2) - B_2(\epsilon_{xy}P_{xy} + \cdots) \ , \qquad (3)$$

where the ϵ's are the symmetrized cubic strain modes. Taking into account the elastic energy when minimizing the free energy leads one to express the ϵ's as functions of the second-order operator's mean values. $\mathcal{H}_{qq}$ and $\mathcal{H}_{\mathrm{me}}$ appear then to have the same form and can be grouped together:

$$\mathcal{H}_{qq} + \mathcal{H}_{\mathrm{me}} = -G_1(\langle O_2^0\rangle O_2^0 + 3\langle O_2^2\rangle O_2^2) - G_2(\langle P_{xy}\rangle P_{xy} + \langle P_{yz}\rangle P_{yz} + \langle P_{zx}\rangle P_{zx}) \ ,$$

with

$$G_1 = K_1 + B_1^2/(C_{11} - C_{12})_0$$

and

$$G_2 = 4K_2 + B_2^2/4(C_{44})_0 \ , \qquad (4)$$

where the C_0's are the background elastic constants without interaction.

All the calculations are made in the fourfold-axes system with a self-consistent method for the eight temperature mean values $\langle J_x\rangle$, $\langle J_y\rangle$, $\langle J_z\rangle$, $\langle O_2^0\rangle$, $\langle O_2^2\rangle$, and different $\langle P_{ij}\rangle$. The three dipole components and the five quadrupole ones are obtained in this axes system. This process allows one to describe the magnetization and magnetostriction mechanisms along the principal crystallographic directions, including the moment rotation when the internal field $\vec{H}_i$ is applied along a hard magnetization axis.

B. Determination of the parameters

We used the preceding formalism for the compound TmZn. In a single domain sample the magnetic moment orders along a fourfold direction, e.g., z, where only $\langle J_z\rangle$ and $\langle O_2^0\rangle$ are present. The $\langle P_{ij}\rangle$ are increasing from zero as soon as the moment is starting away from this direction and the G_2 term contributes then to the Hamiltonian. For simplification we have

studied at first the case $\vec{H}_i$ null or applied along the z axis, where G_2 has no influence. So, four parameters remain to describe the phenomena, namely, W and x defining the cubic paramagnetic level spacing, and B_1 and K_1 included into G_1. The knowledge of the two first ones is provided by the analysis of the neutron spectroscopy spectra.

1. Cubic CEF level scheme

The theoretical aspects for neutron spectroscopy were quoted in previous papers.[4] Calculations are based on the neutron cross section derived by Trammell,[13] where the intensities of transitions are related to the matrix elements between levels.[14] In the fits, besides the CEF parameters, the elastic peak intensity, the spectrometer resolution, and natural transition widths must be taken into account. One major contribution to linewidths at low temperatures is certainly exchange broadening. This contribution within each representation may also lead to a broadening of the quasielastic line, in addition to nuclear incoherent scattering and to the scattering from the cryostat and sample holder. At higher temperatures, an additional term arises from ion-phonon coupling. For sake of simplicity, all the fits are drawn with a constant natural width of 0.5 meV, the most important part being the position and the intensity of the CEF transitions.

A rough analysis of the intense transfers can lead to two solutions on both sides of the $\Gamma_3-\Gamma_5^{(1)}$ crossing in the LLW scheme namely, $x=-0.31$ [$\Gamma_5^{(1)}$ triplet as ground state] or $x=-0.85$ (Γ_3 doublet ground state). Since W is positive, the transfers are then $\Gamma_5^{(1)}-\Gamma_3$ (3.2 meV) and either $\Gamma_5^{(1)}-\Gamma_4$ ($x=-0.31$) or $\Gamma_5^{(1)}-\Gamma_2$ ($x=-0.85$) for the 13.9 meV transfer. But the thermal variation of intensities selects the right solution. If $x=-0.31$, the 13.9 meV line must slightly decrease at 120 K, the Boltzmann factor varying from 97% at 12 K to 48% at 120 K for the $\Gamma_5^{(1)}$ ground state. If $x=-0.85$, its intensity is quite small at 12 K and increases when the $\Gamma_5^{(1)}$ first excited level is populated (6% at 12 K and 50% at 120 K). In addition, the existence at 12 K of the $\Gamma_5^{(1)}-\Gamma_5^{(2)}$ and $\Gamma_5^{(1)}-\Gamma_2$ transfers (respectively, 17.3 and 22.6 meV) leads without ambiguities to the solution ($W=1.2\pm0.1$ K/atom, $x=-0.31\pm0.02$) (inset of Fig. 11). The corresponding CEF parameters are then

$$A_4\langle r^4\rangle=-38.0 \text{ K/atom} ,$$

$$A_6\langle r^6\rangle=-19.6 \text{ K/atom} .$$

The negative signs agree with all the determinations throughout the RZn series. Moreover, the values lie very close to the observed ones in ErZn (-36 and -18 K/atom).[4] Then, we must here reject the level scheme ($W=2.2$ K, $x=-0.8$)[8] previously obtained from the fit of the magnetization curves with only Heisenberg exchange and cubic CEF terms. Note that the corresponding parameters would be

$$A_4\langle r^4\rangle=-170 \text{ K/atom}$$

and

$$A_6\langle r^6\rangle=-10 \text{ K/atom}$$

clearly in disagreement with their variation in RZn series. That shows the importance of the direct determination of the level scheme.

2. Determination of G_1 coefficient

The G_1 term in the Hamiltonian acts only on quadrupolar levels without modification of their intrinsic magnetic moment. In our case, this term must be sufficiently strong to induce at a given temperature T_Q a Jahn-Teller effect splitting the degenerated levels in order to minimize the free energy and causing a spontaneous quadrupolar moment $\langle O_2^0\rangle$ without magnetic ordering. In TmZn, a calculated value of $T_Q=8.6$ K is obtained with $G_1=25.5\pm1$ mK. The magnetic ordering is then predicted occuring in the tetragonal phase for a calculated $T_c=\Theta_p=8.1$ K. Figure 9(a) shows the temperature evolution of the lowest levels below 10 K. In the cubic paramagnetic state the ground level $\Gamma_5^{(1)}$ is composed of a nonmagnetic singlet but with an intrinsic quadrupolar moment ($\langle 1|O_2^0|1\rangle=15$) and of a magnetic and quadrupolar doublet ($\langle 2|gJ_z|2\rangle=-\langle 3|gJ_z|3\rangle=3.15\ \mu_B$ and $\langle 2|O_2^0|2\rangle=\langle 3|O_2^0|3\rangle=-7.5$). At 37 K above, the first excited level Γ_3 is formed of two nonmagnetic but quadrupolar levels ($\langle 4|O_2^0|4\rangle=\langle 5|O_2^0|5\rangle=36$). At T_Q, the Γ_3 doublet is split; the $\Gamma_5^{(1)}$ is decomposed in the degenerated doublet and the nonmagnetic singlet, that is the new ground state. The quadrupolar mean value $Q=\langle O_2^0\rangle$ increases up to 30, according to the purification of the wave functions. A discontinuity on the free energy is observed at T_Q, in agreement with our specific-heat and resistivity data.

At $T_c=8.1$ K, the levels 2 and 3, which could not be separated by G_1, are then split by dipolar exchange; a moment is clearly induced on the nonmagnetic ground-state 1, raising up to 4.5 μ_B at 1 K. Its quick increasing reinforces the Q value, explaining the small taking up reported at T_c on the Q curve. The level splitting is calculated to be continuous at T_c.

We can now come back to the lowest-temperature spectra obtained by neutron spectroscopy. In the paramagnetic tetragonal state, as in the magnetically ordered one, only one collective excitation line has a noticeable intensity involving the five $\Gamma_5^{(1)}$ and Γ_3 levels, that is the longitudinal excitation between 1 and 4 [Fig. 9(a)]. Its energy calculated without q dispersion would reach roughly 25 K, in close agreement with the experimental data (27 K), but without precise three-axes spectrometer experiments no other conclu-

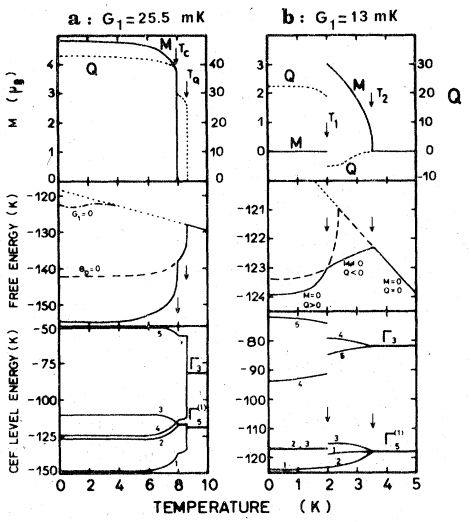

FIG. 9. (a) Calculated temperature variation of the spontaneous magnetization $M = g\langle J_z\rangle$ and quadrupole $Q = \langle O_2^0\rangle$ (high part) of the free energy (middle part, full lines) and of the energy of the CEF levels issued from Γ_3 and $\Gamma_5^{(1)}$ (low part). The parameter values are $W = 1.2$ K, $x = -0.31$, $\Theta_p = 8.1$ K, and $G_1 = 25.5$ mK. Arrows indicate both ordering temperatures T_c and T_Q. In the middle part, dashed lines correspond to $\Theta_p = 0$, $G_1 \neq 0$, semidotted lines to $\Theta_p \neq 0$, $G_1 = 0$, and dotted lines to $\Theta_p = G_1 = 0$. (b) A peculiar case is reported: $\Theta_p = 8.1$ K, $G_1 = 13$ mK, where the most stable configuration changes at $T_1 = 2$ K from a nonmagnetic state toward a magnetic one with a reverse strain (see Sec. III B 3 and Fig. 10).

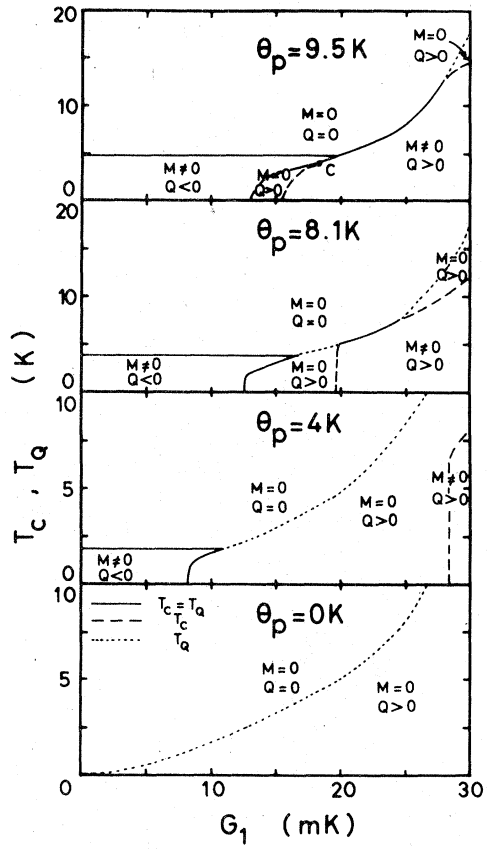

FIG. 10. Variation of T_c, T_Q as a function of G_1 for different values of Θ_p (see Sec. III B 3).

sion can be stated.

As proved by the higher value of T_Q than of T_c, the instability of the cubic phase seems to be the main factor in TmZn. Without the two order terms, the bilinear interactions would split alone the cubic CEF degeneracy, but the same value of $\Theta_p = 8.1$ K would lead to a smaller minimization of the free energy [Fig. 9(a)], the ordering point would be $T_c = 4$ K instead of $T_c = \Theta_p = 8.1$ K.

3. *Interdependence of T_c, T_Q and Θ_p, G_1*

Keeping the MF theory and the simplified harmonic elasticity approximation, we determine the dependence of both order parameters $M = g\langle J_z\rangle$ and $Q = \langle O_2^0\rangle$ on Θ_p and G_1 coefficients. For the range ($0 < \Theta_p < 10$ K, $0 < G_1 < 30$ mK) the main results are reported in the Fig. 10. One can note first different phases depending on Θ_p, G_1 and T. For a given set (Θ_p, G_1, T), our self-consistent process allows sometimes the coexistence of different solutions for the (M,Q) equilibrium values. Thus, $G_1 = 13$ mK, $\Theta_p = 8.1$ K lead to a first-order transition at $T_1 = 2$ K between the two phases ($M = 0$, $Q \sim 22$) and ($M \sim 3$, $Q \sim -5$) and to a second-order one at $T_2 = 3.5$ K toward the cubic paramagnetic configuration [Fig. 9(b)].

For small G_1 values, the most stable state is ($M \neq 0$, $Q \sim -5$). The G_1 effect, favoring the quadrupolar level 1, remains weaker than the Θ_p one, leading to the magnetic level 2 as ground state. Increasing G_1 stabilizes at first the ($M = 0$, $Q \sim 25$) phase, then the ($M \neq 0$, $Q \sim 35$) one. Here, G_1 is strong enough to isolate the nonmagnetic level 1 (first case), but a not too weak Θ_p induces a moment on it (second case). The upper boundary of these two phases coincides with the T_Q curve obtained with $\Theta_p = 0$, that remains stable with regard to Θ_p, even when T_Q and T_c are mixed by a magnetostrictive process. When Θ_p increases, the ($M = 0$, $Q \sim 25$) phase vanishes in favor of the ($M \neq 0$, $Q \sim 35$) one. For high values of Θ_p, the unique phase will be ($M \neq 0$, $Q \sim 35$), the ground state being the level 1, strongly purified to the $J_z = 6$ component. Note that the MF model does not lead here to $T_c = \Theta_p$. T_c varies between 0 and 12 K according to G_1 for $\Theta_p = 8.1$ K, and the calculated value $T_c = \Theta_p$ is certainly a coin-

cidence in TmZn. Indeed the MF model gives equality only for a multiplet with pure $|J_z\rangle$ wave functions. The same case occurs in presence of a CEF level scheme purified by strong magnetic interactions. But if they remain weak in comparison with the level spacing the relation between T_c and Θ_p depends on the CEF configuration.

This phase diagram study leads in the case of TmZn to a very narrow ($M=0$, $Q>0$) phase. That can explain the dependence of the physical properties on the sample preparation as observed on the resistivity measurements.

C. Description of the physical properties

1. Magnetization curves

The field variation of the isothermal magnetization curves along [001] [Fig. 5(b)] and [110] [Fig. 6(b)] is well calculated with $\Theta_p=8.1$ K and $G_1=25.5$ mK, despite a slightly large spontaneous magnetization. In the paramagnetic state, the calculation describes the rapid increasing of the magnetization well for the critical magnetic field H_c, that corresponds to the appearance of the magnetic ordering under the internal field which supplies the exchange interactions. Along the [110] direction the magnetic moment—initially along this direction—turns suddenly at H_c close to the [100] axis then comes again progressively toward the applied field, as in the ordered state. The temperature variation of H_c is satisfactory in our model, chiefly along the fourfold axis [inset Figs. 5(b) and 6(b)]. Finally the same phenomenon exists for $\langle O_2^0\rangle$ variation, as we will see in Sec. III C 2.

We can note that the introduction of the G_2 parameter does not affect the magnetization along [001] but a value $G_2=-70$ mK reduces the moment to 0.3 μ_B at 120 kOe along the hard axes. However, this value cannot be easily confirmed by other methods.

2. Magnetostriction curves

The tetragonal deformation of the crystallographic cell can be written

$$c/a-1=\sqrt{3/2}\,\epsilon_3=\sqrt{3/2}\,[B_1/(C_{11}-C_{12})_0]\langle O_2^0\rangle \quad . \quad (5)$$

From the values of the distortion at 4.2 K, $(-9\pm1)\times10^{-3}$, the background elastic constant

$$(C_{11}-C_{12})_0(1.51\times10^5\ \text{K/atom})$$

and the calculated value of the spontaneous quadrupolar moment (−43) we can deduce the magnitude of the parameter B_1, i.e.,

$$B_1=-25.5\pm1.5\ \text{K/atom}$$

or

$$B_1^2/(C_{11}-C_{12})_0=4.3\pm0.5\ \text{mK} \quad .$$

This B_1 value leads to the calculated strain dependences reported in Fig. 7(b). The strong variation of $\langle O_2^0\rangle$ under field in the paramagnetic state is reproduced by the calculations; the critical field is calculated to be the same as for the magnetization curves, proving that the strengthening of the magnetic interactions by a few kOe applied field induces both orderings simultaneously.

This B_1 value agrees with the determination in the other RZn compounds, according to the variation of $\alpha_j\langle r^2\rangle$ through the series. The biquadratic interaction, calculated from the expression (4), with $G_1=25.5$ mK, reaches $K_1=21.2$ mK and seems then to drive mainly the structural transition. We will compare these conclusions with the ultrasonic data, in Sec. III C 3.

3. Elastic constants

In Ref. 8, we had reported the softening of the $C_{11}-C_{12}$ mode from 300 K down to near 15 K, where the echoes vanished due to the strong ultrasonic attenuation increasing from about 30 K. We had tried to fit with a wrong level scheme ($W=2.2$ K, $x=-0.8$); following many authors[15–19] we had used expression (3) of Ref. 8, where g_2 is proportional to the magnetoelastic coefficient B_1 and g' corresponds to the quadrupolar exchange coupling K_1, χ_s being a strain susceptibility. Written in the linear strain approximation, this simplified expression corresponds then exactly to the present Hamiltonian (Sec. III A). Studying the paramagnetic range allows forgetting any $\vec{J}_i\cdot\vec{J}_j$ contribution.

The χ_s function calculated from the actual level spacing, exhibits an absolute value smaller than previously, then fitting the same data, B_1 and K_1 will be found greater. Another important feature is now a small kink in the 30–40 K range to the Γ_3 position. It is found again in the $C_{11}-C_{12}$ calculated mode (see Fig. 11). The same background for the mode without magnetic interactions than previously takes into account only the isotropic anharmonic terms responsible for the lattice expansion and the C_{ij} thermal dependence at high temperature. We obtain a perfect fit from 300 K down to 40 K with the following values $G_1=20$ mK, $K_1=-20$ mK, ($|B_1|=77$ K/atom with $(C_{11}-C_{12})_0=1.5\times10^5$ K/atom). But below the theoretical kink, the gap increases. The transition temperature is predicted to be $T_{Q\text{calc}}=2$ K. If one wants to extend the fit down to 15 K, it cannot be realized without altering it at high temperature as proved by the variation for $G_1=34$ mK, $K_1=0$ mK, leading to $T_{Q\text{calc}}=4$ K. Such solutions are localized in the (B_1,K_1) plane between (72 K, 0 mK) and (77 K, −20 mK), far from the values obtained in Sec. III C 2 ($G_1=25.5$ mK, $B_1=-25.5$ K, $K_1=21.2$ mK) which lead to a very little softening (10% at 10 K). The assumption of an entirely soft mode, $C(T_Q=8.6\ \text{K})=0$,

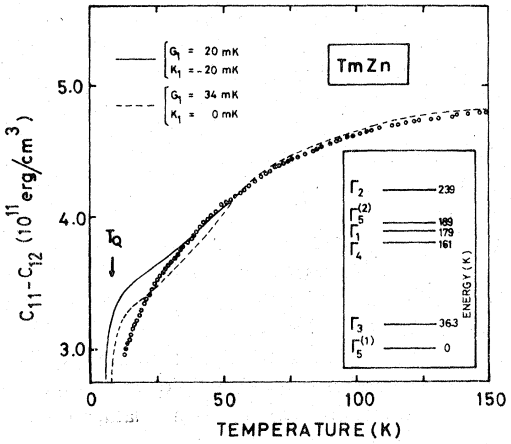

FIG. 11. Experimental and calculated variations of the $C_{11}-C_{12}$ mode at low temperature: full line calculated with $G_1=20$ mK/atom and $K_1=-20$ mK/atom, dashed line with $G_1=34$ mK and $K_1=0$ mK (inset: cubic level spacing).

gives too bad an agreement. That is not surprising because it is well known that for a triplet ground state the mode does not vanish at T_Q.[15,18] In conclusion, if the value of $G_1=B_1^2/C_0+K_1$ does not vary very much between both determinations, the main difference occurs about the various contributions to G_1.

Two additional points should be noted. First, we may not forget the anharmonic terms. They induce the strong energy dissipation below the Jahn-Teller Γ_3 doublet and then modify the sound velocity too, deleting the theoretical kink and removing T_Q. Such an explanation compels us to limit the fit of $C_{11}-C_{12}$ above 40 K. In a more general way, including expressions such as

$$\delta(\epsilon_3^3-3\epsilon_3\epsilon_2^2)-\alpha[(\epsilon_3^2-\epsilon_2^2)O_2^0-2\epsilon_2\epsilon_3O_2^2]\ ,$$

necessitates new experiments in order to determine the supplementary parameters.

On the other hand, the harmonic terms neglected in the $C_{11}-C_{12}$ expression can contribute as assumed by Moran *et al.*[19] and Levy[20] about DySb. Here too, their discussion exceeds the ultrasonic results and involves the used Hamiltonian. In expression (4) of Ref. 19, the first term $g_0^{\alpha 2}$ is our B_1 one; from a pure point-charge model, the following one-ion constants $g_0^{\alpha 4}$ and $g_0^{\alpha 6}$ are found to introduce, respectively, corrections of 5% and 12% on the fourth- and sixth-order CEF parameters.[21,22] But with our knowledge, we cannot predict the strain derivative of CEF parameters any better than the parameters themselves in metallic compounds.

Among the two-ion magnetoelastic terms we have observed the lower-symmetry one, that is the anisotropic bilinear exchange, in isomorphous S-state GdZn, where it drives a tetragonal distortion at T_c ($\epsilon_3\simeq-5\times10^{-4}$ at 4.2 K).[5] If we suppose the same negative coefficient in TmZn, it contributes to ϵ_3 about 8% and must disappear at T_c, like the quadrupolar one at T_Q, neglecting any short range order. The last two $d_0^{\epsilon 4}$, $d_0^{\epsilon 6}$ terms exist in all the thermal range. The fully symmetric $\langle O_4\rangle$ and $\langle O_6\rangle$ average values are temperature dependent. For instance, $\langle O_4\rangle$ exhibits at 40 K a maximum 30% higher than the T_Q value. Below T_Q, they vary strongly (twice for $\langle O_4\rangle$). Such terms may contribute if $d_0^{\epsilon 4}$ and $d_0^{\epsilon 6}$ are not too weak.

Thus, in addition to the anharmonicity, all the high-order harmonic terms can modify the free energy, the phase diagram, and the calculated physical properties. The low-temperature determination of G_1 without anharmonic terms may be too rough a simplification. Third-order elastic constants experiments appear to be rich in information.

IV. CONCLUSION

The main result of our study lies in the fact that TmZn is a Jahn-Teller system and not a magnetostrictive one. It differs thus from the other RZn compounds, where the $\vec{J}_i\cdot\vec{J}_j$ interactions are predominant. For instance the Heisenberg contribution

$$[3\Theta_p/J(J+1)]\langle J_z\rangle^2$$

is more than 30 K/atom in ErZn. The biquadratic and magnetoelastic terms are then perturbations (3.6 K/atom) and the lattice distortion is driven by the magnetic ordering.[5] In TmZn the dipolar energy (3.8 K) is clearly lower than the other contributions (see Table I) and the influence of the neglected terms can become more drastic. TmZn is then more like the isomorphous TmCd.[9] However, in this latter compound, no magnetic ordering has been observed whereas it appears below T_Q in TmZn. We may regret that in TmZn the two ordering points are too close to each other, constraining the study of the paramagnetic tetragonal phase. In addition, the TmZn value $G_1=25.5$ mK is stronger than the TmCd one ($G_1=1.7$ mK).[9]

It appears that in TmZn a single experiment such as elastic constants or magnetization measurements is not sufficient to give a good knowledge of all the necessary parameters. It is then of primary importance to obtain the CEF ones by a direct determination. For instance, the level scheme defined by $W=2.2$ K, $x=-0.8$ would allow a very nice and complete interpretation of all the data without any suspicion about the validity of the used formalism. But the neutron spectroscopy provides without ambiguities the actual level scheme corresponding to CEF parameters in agreement with those observed throughout the RZn series.

If the chosen Hamiltonian with its approximations

TABLE I. Comparison of some physical constants and energies between TmZn and TmCd compounds.

	TmZn	TmCd
T_Q (K)	8.55	3.16[a]
T_c (K)	8.12	<0.04[a]
$10^3(c/a-1)$	-9 ± 1	-0.6[b]
W (K/atom)	-1.21 ± 0.1	
x	0.31 ± 0.02	
G_1 (mK/atom)	25 ± 10	1.3[a]
$B_1^2/(C_{11}-C_{12})_0$ (mK/atom)	$+6.4\pm0.5$ from ϵ_3 data	0.4[a]
Heisenberg dipolar exchange (K/atom)	3.8	0
Quadrupolar exchange (K/atom)	35 with $K_1=19$ mK	2.4
Magnetoelastic energy (K/atom)	11.8 ± 2 from ϵ_3 data	0.7

[a]Reference 9.
[b]Reference 23.

appears to describe the results accurately, however, one may keep in mind the limits of the MF model about the magnetic excitations which would be better treated in the random-phase approximation. That could reduce, for instance, the calculated moment. Due to the strong value of the distortion the neglected terms, in particular the anharmonic ones, may contribute and have now to be evaluated. Other obscurities remain. One is the interaction mechanism between the $4f$ quadrupoles. Another is a proper microscopic analysis of the magnetoelastic coefficients. Here it will be necessary to calculate the CEF parameters and their strain modification.

Note added in proof: Current studies of elastic constants reveal that theoretical fits based on this harmonic elasticity model are better than those in Sec. III C 3: the B_1 and K_1 values from Sec. III C 2 are found again.

ACKNOWLEDGMENTS

We thank A. de Combarieu and E. Bedin (Service des Basses Températures of the Nuclear Center of Grenoble) for their aid in the specific-heat experiments. The contribution of Dr. A. Murani and Dr. P. Lethuillier in connection with neutron-spectroscopy and resistivity measurements, respectively, is also gratefully acknowledged. Stimulating discussions with Professor B. Lüthi have been strongly appreciated.

[1]A. Iandelli and A. Palenzona, J. Less Common Metals 9, 61 (1965); K. Kanematsu, G. T. Alfieri, and E. Banks, J. Phys. Soc. Jpn. 26, 244 (1969).
[2]P. Morin and J. Pierre, Solid State Commun. 13, 537 (1973); Phys. Status Solidi A 17, 479 (1973).
[3]P. Morin and A. De Combarieu, Solid State Commun. 17, 975 (1975); P. Morin, J. Pierre, and J. Chaussy, Phys. Status Solidi A 24, 425 (1974).
[4]P. Morin, J. Pierre, J. Rossat-Mignod, K. Knorr, and W. Drexel, Phys. Rev. B 9, 4932 (1974); P. Morin, J. Pierre, D. Schmitt, and W. Drexel, J. Phys. (Paris) 37, 611 (1976); D. Schmitt, P. Morin, and J. Pierre, Phys. Rev. B 15, 1698 (1977).
[5]P. Morin, J. Rouchy, and E. Du Tremolet De Lacheisserie, Phys. Rev. B 16, 3182 (1977).
[6]M. Belakhovsky and D. K. Ray, Phys. Rev. B 12, 3956 (1975).
[7]J. Pierre, D. Schmitt, P. Morin, and B. Hennion, J. Phys. F 7, 1965 (1977).
[8]P. Morin, A. Waintal, and B. Lüthi, Phys. Rev. B 14, 2972 (1976).
[9]B. Lüthi, M. E. Mullen, K. Andres, E. Bucher, and J. P. Maita, Phys. Rev. B 8, 2639 (1973).
[10]H. Taub, S. J. Williamson, Solid State Commun. 13, 1021 (1973).
[11]K. R. Lea, M. J. M. Leask, and W. P. Wolf, J. Phys. Chem. Solids 23, 1381 (1962).
[12]J. Sivardiere, J. Magn. Magn. Mater. 1, 23 (1975).
[13]G. T. Trammell, Phys. Rev. 92, 1387 (1953).
[14]R. J. Birgeneau, J. Phys. Chem. Solids 33, 59 (1972).
[15]M. Kataoka and J. Kanamori, J. Phys. Soc. Jpn. 32, 113 (1972).
[16]G. A. Gehring and K. A. Gehring, Rep. Prog. Phys. 38, 1 (1975).
[17]M. E. Mullen, B. Lüthi, P. S. Wang, E. Bucher, L. D. Longinotti, J. P. Maita, and H. R. Ott, Phys. Rev. B 10, 186 (1974).
[18]Y. Kino, B. Lüthi, and M. E. Mullen, J. Phys. Soc. Jpn. 33, 687 (1972).
[19]T. J. Moran, R. L. Thomas, P. Levy, and H. H. Chen, Phys. Rev. B 7, 3238 (1973).
[20]P. Levy, J. Phys. C 6, 3545 (1973).
[21]B. Lüthi, P. S. Wang, Y. H. Wong, H. R. Ott, E. Bucher, *Crystal Field Effects in Metals and Alloys*, edited by A. Furrer (Plenum, New York, 1977).
[22]F. Levy, Phys. Kondens. Mater 10, 86 (1969).
[23]H. R. Ott and K. Andress, Solid State Commun. 15, 1341 (1974).